THE JOURNAL OF PHYSICAL CHEMISTRY A

ARTICLE

pubs.acs.org/JPCA

# Structure of the Aqueous Electron: Assessment of One-Electron Pseudopotential Models in Comparison to Experimental Data and Time-Dependent Density Functional Theory

John M. Herbert* and Leif D. Jacobson†

Department of Chemistry, The Ohio State University, Columbus, Ohio 43210, United States

**ABSTRACT:** The prevailing structural paradigm for the aqueous electron is that of an *s*-like ground-state wave function that inhabits a quasi-spherical solvent cavity, a viewpoint that is supported by numerous atomistic simulations using various one-electron pseudopotential models. This conceptual picture has recently been challenged, however, on the basis of results obtained from a new electron−water pseudopotential model that predicts a more delocalized wave function and no well-defined solvent cavity. Here, we examine this new model in comparison to two alternative, cavity-forming pseudopotential models. We find that the cavity-forming models are far more consistent with the experimental data for the electron's radius of gyration, optical absorption spectrum, and vertical electron binding energy. Calculations of the absorption spectrum using time-dependent density functional theory are in quantitative or semiquantitative agreement with experiment when the solvent geometries are obtained from the cavity-forming pseudopotential models, but differ markedly from experiment when geometries that do not form a cavity are used.

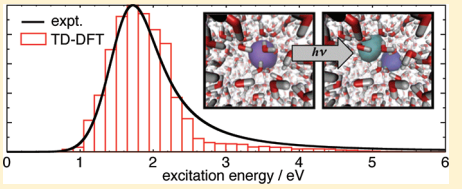


## 1. INTRODUCTION

The aqueous electron, $e^-(aq)$, has attracted significant attention from both theory and experiment[1−3] ever since it was first observed in 1962.[4,5] At a practical level, this species is an important intermediate in the radiation chemistry of aqueous systems,[1,6] but it is also an intriguing problem in fundamental chemical physics. As a charged species, the electron experiences strong interactions with water molecules and, according to certain theoretical models, is capable of forming ion−water hydrogen bonds. At the same time, $e^-(aq)$ is fundamentally a solvent-supported ion insofar as $H_2O^-$ does not exist,[7] and numerous water molecules are required in order to reproduce the properties of bulk $e^-(aq)$.[2,8,9] Furthermore, the lack of a nuclear center binding the unpaired electron means that the $e^-(aq)$ wave function is quite polarizable, and electron−water dispersion interactions are thought to contribute significantly to the stabilization of this species.[2,10,11]

Alternatives to a strictly one-electron "charge defect" (or "color center") explanation for the structure of $e^-(aq)$, or whatever species is responsible for absorption at 720 nm following water radiolysis, have been proposed over the years. These include molecular models involving an $OH^-\cdots H_3O$ complex,[12,13] a hydrated $H_3O$ radical,[14−18] or a solvent/anion complex.[19,20] Although these alternative models have been criticized for being inconsistent with experimental spectroscopy,[3,21] certain aspects of them may warrant further theoretical consideration. However, the purpose of the present work is to examine various one-electron models of $e^-(aq)$ in which this species is assumed to be a negative charge defect in liquid water.

The dominant theoretical paradigm for understanding the structure of $e^-(aq)$, dating back to the earliest theoretical models of this species,[22−24] is one in which a quasi-spherical, *s*-type ground-state wave function occupies a void within the solvent, as depicted in Figure 1a. This viewpoint is supported by numerous atomistic simulations that have been performed over the past 25 years,[25−45] including all-electron density functional theory calculations.[45]

Ab initio studies of $e^-(aq)$ are expensive because at least two solvation shells are required to support a cavity-bound electron,[2] and the binding motifs that are obtained in finite cluster studies are quite sensitive to the temperature and the manner in which the clusters are prepared.[48−51] As such, the primary simulation tools for describing $e^-(aq)$ have been one-electron models in which the water molecules are described using a force field, and only the unpaired electron is described by a wave function. The key ingredient in such models is an electron−water pseudopotential. Unfortunately, $e^-(aq)$ properties are sometimes sensitive to subtle features of this pseudopotential.[2,44,46]

The newest of these electron−water pseudopotentials was developed recently by Larsen, Glover, and Schwartz (LGS).[46] Unlike previous one-electron models,[32−34,41,44] the LGS model exhibits the unusual feature that the ground-state wave function does not carve out a well-defined solvent cavity (see Figure 1b), and on the basis of simulations using this model, LGS have questioned the veracity of the cavity model of $e^-(aq)$.[46,52] The LGS model reproduces several observed features of $e^-(aq)$, including its diffusion constant, radius of gyration, electronic absorption maximum, and lack of observable polarization anisotropy in transient hole-burning experiments.[46] At the same time, most of these features are reproduced equally well by the

**Received:** July 6, 2011
**Revised:** October 21, 2011
**Published:** October 27, 2011

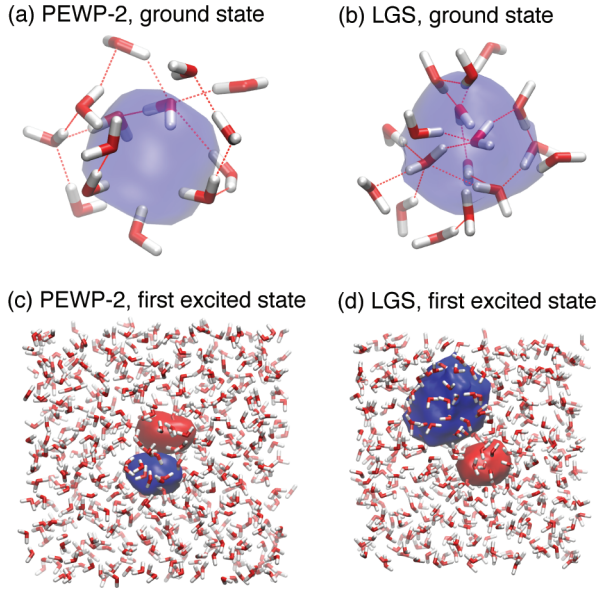


**Figure 1.** Representative images of the ground-state and first excited-state wave functions for $e^-$(aq), obtained from the cavity-forming "PEWP-2" pseudopotential model[44] and from the non-cavity-forming Larsen–Glover–Schwartz (LGS) pseudopotential model.[46] (Wave functions obtained from the cavity-forming Turi–Borgis model[41] and the non-cavity-forming LGS-mPol model[47] are not shown, as they are qualitatively similar to the PEWP-2 and LGS wave functions, respectively.) Isosurfaces depicted here encapsulate 70% of $|\psi|^2$. In panels (a) and (b), all water molecules within 4.5 Å of the centroid of $\psi$ are shown, whereas panels (c) and (d) depict the entire simulation cell, which contains 600 water molecules in (c) and 499 molecules in (d).

cavity-forming models,[41,43,44,53,54] and various technical aspects of the LGS model have been criticized.[47,64]

Here, we report new simulations using the LGS pseudopotential model and compare the results to two alternative, cavity-forming, one-electron models.[41,44] The latter are found to afford much better agreement with experimental data for the vertical electron binding energy (VEBE), the electronic absorption spectrum, and the electron's radius of gyration. In addition, we find that the agreement between experiment and LGS predictions deteriorates, for certain observables, when Ewald summation is used to evaluate the long-range Coulomb interactions, rather than the minimum-image convention that has been used in all previous LGS simulations.

We also report time-dependent density functional theory (TD-DFT) calculations of the $e^-$(aq) absorption spectrum, using a carefully calibrated quantum mechanics/molecular mechanics (QM/MM) methodology based on solvent configurations extracted from the one-electron pseudopotential simulations. Quantitative or semiquantitative agreement with the experimental spectrum is observed when the cavity-forming geometries are used, whereas the spectrum simulated using LGS geometries lies far to the red of the experimental spectrum. In our view, these TD-DFT calculations provide the most compelling evidence to date in favor of the cavity-forming pseudopotential models.

The remainder of this work is organized as follows. Section 2 provides a brief overview of the three different one-electron pseudopotential models that are examined here. The predictions of these models (for the electron's radius of gyration, VEBE, and optical spectrum) are examined in section 3. TD-DFT calculations are discussed in section 4. Finally, section 5 summarizes the current state of affairs with regard to benchmark data for one-electron pseudopotential models of $e^-$(aq).

## 2. SIMULATIONS

Several different one-electron pseudopotential models are examined herein, including the LGS model[46] (already mentioned above); the Turi–Borgis (TB) model,[41] which is formally similar in some respects but employs a different electron–water pseudopotential; and also a polarizable model that we have recently developed.[44] The mathematical structure of these models is briefly reviewed in section 2.1, and then in section 2.2 we provide details regarding how the condensed-phase $e^-$(aq) simulations were performed.

**2.1. One-Electron Pseudopotential Models.** The LGS and TB models of the hydrated electron bear some formal similarity with one another, even though their physical predictions differ markedly. In particular, both models employ the nonpolarizable "simple point charge" (SPC) force field for water,[65] and both use a one-electron Hamiltonian of the form

$$\hat{H}(\vec{r}) = -\frac{\hbar^2}{2m_e}\hat{\nabla}_r^2 + \sum_J^{N_{water}}\left[V_{e-water}(\vec{r},\vec{R}_J) + \sum_{K>J}^{N_{water}} V_{SPC}(\vec{R}_J,\vec{R}_K)\right] \quad (1)$$

The symbol $\vec{R}_J$ denotes a collective set of coordinates for the $J$th water molecule. These coordinates serve as parameters in the one-electron Schrödinger equation, $\hat{H}|\psi\rangle = E|\psi\rangle$, and we propagate classical molecular dynamics for the water molecules along the ground-state eigenvalue, $E = E(\{\vec{R}_J\})$, using Hellmann–Feynman forces.[66]

The electron–water interaction potential, $V_{e-water}$, consists of several components,

$$V_{e-water} = V_{pseudo} + V_{Coulomb} + V_{pol} \quad (2)$$

Here, $V_{Coulomb}$ denotes the Coulomb interaction between the electron and the SPC atomic point charges, while

$$V_{pol}(\vec{r},\vec{R}_J) = \left[\frac{-\alpha}{2(|\vec{r}-\vec{R}_J|^2 + C)^2}\right] f(|\vec{r}-\vec{R}_J|) \quad (3)$$

is an ad hoc electron–water polarization potential of the sort used in many previous studies.[67,68] We use the notation $|\vec{r}-\vec{R}_J|$ in eq 3 to denote the distance between the electron and whatever water site is chosen as the origin for $V_{pol}$. The quantity $\alpha$ is the spherically averaged polarizability of $H_2O$, $f$ is a damping function,[67] and $C$ is a constant whose role in approximating more sophisticated polarization potentials has been discussed previously.[66] [Note that $C = 0$ for the LGS model, and $f \equiv 1$ for the TB model; eq 3 is used for generality.]

The final component of $V_{e-water}$, and the one that proves to be crucial in determining the qualitative nature of the model, is an electron–water pseudopotential, $V_{pseudo}$, and this is where the TB and LGS models differ substantively. Of the various electron–water pseudopotentials in the literature,[2] we have chosen the TB model[41] as a representative example of a nonpolarizable, cavity-forming pseudopotential model because it has been used in many recent simulations of both $e^-$(aq) and finite water cluster anions.[41,42,69−75] Both the LGS and the TB forms of $V_{pseudo}$ are based on a frozen-core Hartree–Fock description of $H_2O^-$, and are attempts to develop a pseudopotential, $V_{pseudo}(\vec{r})$,


dx.doi.org/10.1021/jp206391d | J. Phys. Chem. A 2011, 115, 14470–14483

that reproduces the asymptotic behavior of the Hartree−Fock singly occupied molecular orbital (SOMO). However, the TB and LGS fitting procedures (and, thus, the pseudopotentials themselves) differ in important details, as described in ref 52. Evidently, these details are enough to afford qualitative differences in the structure of $e^-$(aq); the TB model localizes the ground-state wave function into a well-defined solvent cavity in a manner similar to what is depicted for the PEWP-2 ground-state wave function in Figure 1a, whereas no solvent cavity is obtained with the LGS model.

In previous work,[47] we showed that the LGS model overestimates VEBEs of $(H_2O)_n^-$ clusters, as compared to ab initio benchmarks, and that much more accurate VEBEs could be obtained by modifying the parameter $C$ appearing in the ad hoc polarization potential of eq 3. We obtained a modified value of $C$ by fitting to an extensive database of VEBEs without otherwise modifying the LGS model of $e^-$(aq), and we called this variant the "LGS-mPol" (for "modified polarization") model.[47] Although LGS-mPol was never intended as a serious model of the hydrated electron, it does provide an interesting comparison insofar as it uses the same pseudopotential as the LGS model but a different polarization potential.

In addition to these three SPC-based models, we also consider a polarizable model that we have recently developed.[44] Instead of SPC, our hydrated-electron model uses the AMOEBA force field for water,[76,77] in which polarization is described by inducible point dipoles, $\vec{\mu}_i^{\,\mathrm{ind}}$. These dipoles are electronic degrees of freedom, and our model treats them as variables (rather than parameters) in the Hamiltonian. As such, both water−water and electron−water polarization are treated self-consistently in our model. The Hamiltonian has a similar structure to that given in eq 1, with $V_{\mathrm{AMOEBA}}$ replacing $V_{\mathrm{SPC}}$, and with electron−water Coulomb interactions, $V_{\mathrm{Coulomb}}$, that now include interactions with both the permanent $H_2O$ multipoles (charges, dipoles, and quadrupoles in the AMOEBA model), as well as the inducible dipoles. Interactions between the QM electron and the classical induced dipoles naturally furnishes a *many-body* electron−water polarization potential, so there is no need for the ad hoc two-body polarization potential of eq 3.

The induced dipoles are determined by the equation

$$\vec{\mu}_i^{\,\mathrm{ind}} = \alpha_i\left(\vec{F}_i^{\,\mathrm{QM}} + \vec{F}_i^{\,\mathrm{MM}}\right) \tag{4}$$

where $\alpha_i$ is the polarizability of the $i$th atomic site.[78,76] The quantities $\vec{F}_i^{\,\mathrm{QM}}$ and $\vec{F}_i^{\,\mathrm{MM}}$ are the electric fields at the $i$th site that originate from the wave function and from the water molecules, respectively. Because $\vec{F}_i^{\,\mathrm{QM}}$ depends on the $e^-$ wave function and $\hat{H}$ depends on the induced dipoles, eq 4 is coupled to the Schrödinger equation, and these two equations must be iterated to self-consistency. Details of this procedure can be found in our previous papers.[44,66]

As with the nonpolarizable models, a key aspect of our polarizable electron−water potential (PEWP) is the electron−water pseudopotential, $V_{\mathrm{pseudo}}$. Here, we utilize "version 2" of our pseudopotential (PEWP-2),[44] which was parametrized in a manner similar to how the TB pseudopotential was developed. (Indeed, the TB and PEWP-2 pseudopotentials are rather similar when plotted in real space.[44]) We have shown previously[2,43,44] that the PEWP-2 model reproduces and rationalizes a wide variety of experimental data for $e^-$(aq), including the vertical electron binding energy and optical absorption spectrum.[43,44] This model also provides a tentative explanation for other features of $e^-$(aq) that have been inferred indirectly, including large-amplitude librational dynamics in the first solvation shell (which has been inferred based on resonance Raman spectroscopy[21]), as well as the absence of any detectable polarized transient hole-burning dynamics.[79]

**2.2. Simulation Protocols.** We simulate $e^-$(aq) in bulk water by propagating classical molecular dynamics for the water molecules on the lowest adiabatic potential surface of the one-electron Schrödinger equation. This equation is solved on a real-space grid, as described in ref 44, and in the case of the PEWP-2 model it must be solved iteratively along with eq 4 for the induced dipoles. A key aspect of the present simulations, as compared to previous $e^-$(aq) simulations using the LGS model,[46,47,52] is the use of Ewald summation for the long-range electrostatic interactions, whereas previous studies employed the minimum-image convention. This primarily affects the VEBE but has some impact on the radius of gyration and the optical spectrum as well. Both the minimum-image and Ewald summation results are compared below in the case of the LGS model.

Simulations using the LGS model were carried out in a cubic simulation cell containing 499 water molecules (box length $L$ = 24.64 Å), corresponding to a water density of 0.997 g/cm$^3$. TB and PEWP-2 simulations were performed at the same water density but with $L$ = 26.2015 Å and 600 water molecules in the unit cell. (These simulations were taken from ref 44, to which the reader is referred for details.) The TB and PEWP-2 simulations used a grid spacing of $\Delta x$ = 0.93 Å, consistent with our previous work,[44] but the LGS results are somewhat more sensitive to the grid spacing, and for these simulations we use $\Delta x$ = 0.59 Å, as in ref 46. Following Larsen et al.,[46] we use a 32 × 32 × 32 grid (18.17 Å on a side) to simulate the ground-state dynamics. To compute excited states, however, we use a 42 × 42 × 42 grid (24.05 Å on a side), which essentially fills the simulation cell.

All simulations are carried out in the canonical (NVT) ensemble, using Nosé-Hoover thermostat chains at $T$ = 298 K. Larsen et al.[46] employ a time step of 0.5 fs, and for LGS simulations using the minimum-image convention, we follow this practice. However, due to the additional expense of summing the long-range interactions via regular Ewald summation, we explored the use of a 1.0 fs time step for simulations that employ Ewald summation. We find that the extended-system energy (Nosé-Hoover conserved quantity) is well conserved, even for the larger time step. An LGS/Ewald simulation of 35 ps in length, using a 1.0 fs time step, and another simulation of 30 ps in length with a 0.5 fs time step, were combined for the purpose of analysis. LGS/minimum-image simulations were run for 30 ps.

Each optical absorption spectrum is computed using at least 400 snapshots extracted from the ground-state molecular dynamics simulation at intervals of 75−150 fs. For each of these snapshots, we compute the lowest 30 electronic states, then construct a spectrum from a histogram of excitation energies weighted by oscillator strengths, $f_{0\to n}$, where[80]

$$f_{0\to n} = \frac{2m_e}{3\hbar^2}\left(E_n - E_0\right)\sum_{\kappa\,\in\,\{x,y,z\}}\left|\langle\psi_0|\hat{\kappa}|\psi_n\rangle\right|^2 \tag{5}$$

For the PEWP-2 model, the treatment of the solvent's polarization response (i.e., changes in the induced dipoles following excitation of the wave function) is not straightforward. We have addressed this issue elsewhere,[81] where we have shown that similar spectra are obtained using perturbative versus

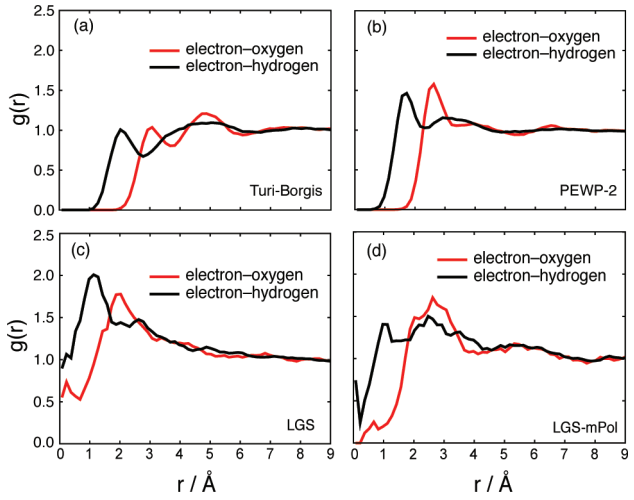


**Figure 2.** Radial distribution functions (RDFs) for (a) the TB model, (b) the PEWP-2 model, (c) the LGS model, and (d) the LGS-mPol model, using Ewald summation in each case. The TB and PEWP-2 models are cavity-forming and their RDFs exhibit shell structure, whereas such structure is largely absent in the two LGS-based models.

self-consistent relaxation techniques. As such, the perturbative technique described in ref 44 is used exclusively here.

## 3. RESULTS FROM PSEUDOPOTENTIAL SIMULATIONS

**3.1. Structure.** The most salient difference between the LGS model and most other one-electron pseudopotential models is that the former fails to localize the ground-state electron in a well-defined solvent cavity, as illustrated in the snapshot of the ground-state wave function that is depicted in Figure 1b, which shows water molecules permeating throughout the $e^-$ wave function. One should bear in mind that, even for cavity-forming models, the tail of the wave function penetrates into the second solvation shell;[11,43,44] hence, a better illustration of the noncavity nature of the LGS electron is obtained by examining radial distribution functions (RDFs), $g(r)$, which are shown in Figure 2. (To compute a classical RDF for this system, we take the electron's position to be the centroid of its wave function.) The TB and PEWP-2 models exhibit an unmistakable shell structure, and furthermore, $g(r) = 0$ for any electron−hydrogen distance smaller than about 1 Å, which provides an indication of the size of the solvent cavity predicted by these two models. In contrast, the LGS model affords electron−hydrogen and electron−oxygen RDFs that are both finite at $r = 0$, and no well-defined shell structure is evident in either RDF. The same is true of the LGS-mPol model, which differs from LGS only in the form of the long-range polarization potential.

Despite the obvious differences in their wave functions and RDFs, the TB and LGS models are reported to afford similar values for the radius of gyration, $r_g$, defined as

$$r_g = \langle\psi|(\vec{r} - \vec{r}_{avg})\cdot(\vec{r} - \vec{r}_{avg})|\psi\rangle^{1/2} \quad (6)$$

where $\vec{r}_{avg} = \langle\psi|\vec{r}|\psi\rangle$. Ensemble-averaged values of $r_g$, which we denote as $\langle r_g\rangle$, are reported in Table 1. The TB model affords $\langle r_g\rangle = 2.42$ Å, in excellent agreement with the value extracted from a moment analysis of the experimental optical absorption line shape ($\langle r_g\rangle = 2.44$ Å).[9] The LGS model affords similarly good agreement ($\langle r_g\rangle = 2.46$ Å) when the minimum-image convention is used to sum the Coulomb interactions. This agreement was put forth in ref 46, as evidence that the noncavity LGS model is at least plausible. However, we find that the LGS value for $\langle r_g\rangle$ increases to 2.69 Å when Ewald summation is used to sum the long-range interactions. The PEWP-2 model errs in the other direction and predicts a $r_g$ that is about 0.2 Å too small.

**Table 1. Ensemble-Averaged Radius of Gyration and VEBE for $e^-$(aq) at $T$ = 298 K and Normal Water Density**

| | | | ⟨VEBE⟩/eV | | |
|---|---|---|---|---|---|
| model | protocol | $\langle r_g\rangle$/Å | unrelaxed | relaxed[a] | extrapolated[b] |
| TB | Ewald | 2.42 | 3.85 | 2.55 | 3.50 |
| PEWP-2 | Ewald | 2.25 | 4.37 | 3.35 | 3.70 |
| LGS | min. image | 2.46 | 5.19 | | |
| LGS | Ewald | 2.69 | 6.29 | | |
| LGS-mPol | min. image | 2.74 | 3.82 | | |
| experiment | | 2.44[c] | | 3.4 ± 0.2[d] | |
| | | | | 3.4, 4.0[e] | |

[a] Includes electronic relaxation of the solvent, estimated in various ways (see section 3.2). [b] Relaxed VEBE, extrapolated to the infinite-dilution limit. [c] From moment analysis of the absorption spectrum at $T$ = 298 K.[9] [d] From liquid microjet measurements.[3,82−85] [e] From extrapolations of cluster photoelectron data.[9,86]

**3.2. Vertical Electron Binding Energy.** Experimental estimates for the VEBE of $e^-$(aq) in bulk water range from 3.3−4.0 eV.[3] This range includes a value of 3.4 eV extrapolated from the photoelectron spectra of warm $(H_2O)_n^-$ clusters,[9] a value of ≈4.0 eV extrapolated from cold cluster data,[86] and four different liquid microjet measurements,[82−85] all of which lie within the range 3.4 ± 0.2 eV. (See ref 3 for a review of the microjet experiments.) Ensemble-averaged VEBEs for the bulk species, as computed from the pseudopotential simulations, are reported in Table 1.

For the TB and PEWP-2 models, we report three different values of the bulk VEBE in Table 1: relaxed, unrelaxed, and extrapolated. The "unrelaxed" VEBE is computed using our 600-molecule simulation cell with proper account of periodic boundary conditions but without modifying the solvent dipoles upon electron detachment in the case of the PEWP-2 model. The "relaxed" VEBE corrects this unrelaxed value by considering electronic reorganization of the solvent upon electron detachment. For the PEWP-2 model, this correction is computed explicitly by relaxing the induced dipoles following electron detachment, whereas for the TB model, we estimate this correction using a continuum model[87] that employs the solvent's optical dielectric constant, $\varepsilon_\infty$, along with parameters $\langle r_g\rangle$ and $\langle T\rangle$ that are extracted from the simulations, to estimate electronic relaxation. (Details can be found in ref 44, where we demonstrate that both the continuum model and the explicit many-body treatment of polarization afford similar electronic relaxation energies.) Finally, the "extrapolated" VEBE reported in Table 1 represents the relaxed VEBE extrapolated to the infinite-dilution ($L \rightarrow \infty$) limit.

Comparison of the aforementioned values demonstrates that both the correction for electronic relaxation as well as the correction for finite simulation cell size are greater than 1 eV in magnitude, even for the large simulation cells that are used here. However, the two corrections differ in sign. If both effects are

ignored, then the TB value for the bulk VEBE (3.85 eV) is deceptively reasonable. However, extrapolation to the infinite-dilution limit without correcting for electronic relaxation yields an unreasonably large VEBE (4.8 eV), while the relaxation correction, when applied without extrapolation, affords an unreasonably small VEBE (2.55 eV). When *both* corrections are applied, the TB and the PEWP-2 models both afford VEBEs within the range of experimental estimates.

For the LGS model, we report only the unrelaxed and nonextrapolated VEBE. Even so, the overbinding character that we previously documented[47] in $(H_2O)_n^-$ cluster VEBEs is reflected in the bulk value as well. Although we have noted this before,[47] based on $e^-(aq)$ simulations performed within the minimum-image convention, here we discover that Ewald summation increases the bulk VEBE by a further 1.1 eV, to 6.3 eV. (This observation is not unique to the LGS model; Ewald summation increases the VEBE for the TB model by 0.8 eV relative to the minimum-image result.[73]) The LGS model is not polarizable, but it is not obvious that the Born-type continuum model that we used to estimate electronic relaxation in the TB case is appropriate when the electron is not localized in a cavity. That said, even the largest, bulk-extrapolated estimate of the electronic relaxation that we saw in our previous work,[44] 1.4 eV, would reduce the LGS value of the VEBE only to 4.9 eV, and subsequent extrapolation to the infinite-dilution limit would most likely afford a VEBE $\gg$ 4.9 eV, far beyond the range of experimental estimates.

Interestingly, the LGS-mPol model affords an unrelaxed and nonextrapolated VEBE that is quite close to the corresponding TB value. This is consistent with the fact that statistical errors for $(H_2O)_n^-$ cluster VEBEs are quite similar for the TB and LGS-mPol models[88] and suggests that a more sophisticated form of the long-range polarization potential might correct the serious overbinding that is exhibited by LGS-type models.[91] We have not pursued such a strategy here.

**3.3. Optical Absorption Spectrum.** Perhaps the most important experimental observable for $e^-(aq)$, from a utilitarian point of view, is its optical absorption spectrum, because this is the principle means by which this species is detected and monitored. Because $e^-(aq)$ absorbs in a relatively uncongested region of the spectrum, its optical absorption (which peaks at 1.7 eV or 720 nm, under ambient conditions[9]) is often used to monitor the kinetics of water radiolysis experiments. Furthermore, the optical spectrum of $e^-(aq)$ has long been used to validate one-electron models of this species, even though most of these models do a poor job of reproducing the overall experimental line shape.[92] We have recently shown[43,44,81] that repolarization of the solvent in response to excitation of the wave function, which is missing from most one-electron models, is the key to obtaining a "blue tail" in the absorption line shape, as is observed experimentally.[9]

The absorption spectra of finite $(H_2O)_n^-$ clusters, as well as that of $e^-(aq)$ under various thermodynamic conditions, are fit very well by a line shape function, $I(E)$, that is a Gaussian on the red side of the spectrum and a Lorentzian on the blue side:[9,93]

$$I(E) = \begin{cases} A \exp[-(E - E_{max})^2/2\sigma_G^2] & \text{if } E \leq E_{max} \\ A[1 + (E - E_{max})^2/\sigma_L^2]^{-1} & \text{if } E > E_{max} \end{cases} \quad (7)$$

We eliminate the parameter $A$ by normalizing the peak absorbance to unity, leading to a three-parameter fit. Temperature-dependent fits of the line shape parameters $E_{max}$, $\sigma_G$, and $\sigma_L$ for the bulk species have been reported by Coe et al.,[9] and these line shape parameters (at $T$ = 298 K) are used to plot the experimental absorption spectrum in the comparisons that follow.

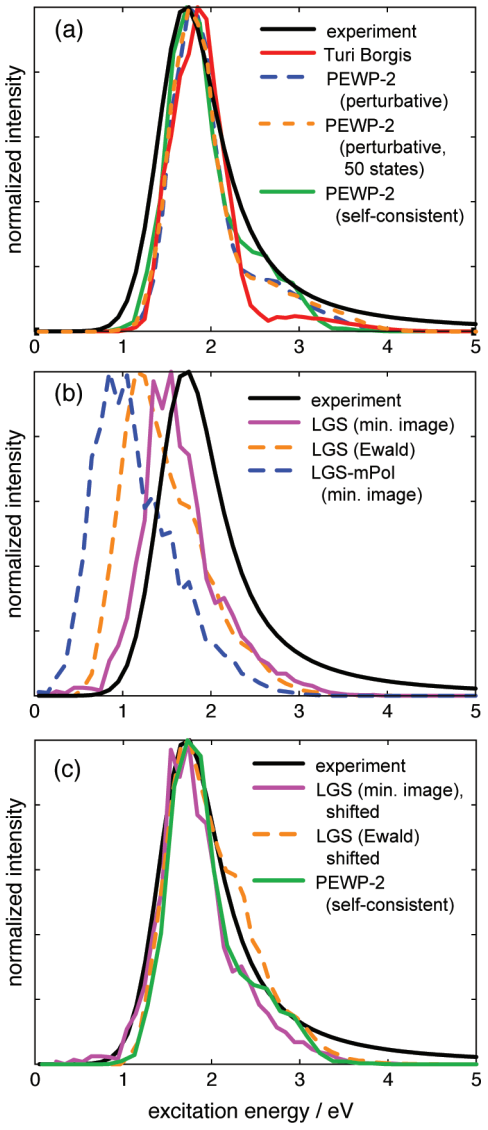


**Figure 3.** Optical spectra of $e^-(aq)$ simulated using a variety of one-electron models. In panel (a), two different methods are compared for computing electronic relaxation in the PEWP-2 model, namely, second-order perturbation theory[43,44] (where we show results including either 30 or 50 excited states) and also a self-consistent procedure.[81] Panel (b) shows the optical spectrum computed using LGS-based models. In panel (c), shifted versions of the LGS spectra are compared to the unshifted PEWP-2 result. Except where indicated, all calculations employ 30 electronic states.

From the earliest atomistic simulations of $e^-(aq)$, the Gaussian feature in the absorption spectrum has been explained in terms of three $s \rightarrow p$ excitations of an electron in a quasi-spherical solvent cavity.[33,36,37] The Lorentzian tail on the blue side of the spectrum, however, is absent in the spectra computed using nearly all one-electron pseudopotential models.[92] Given that the photoelectron spectrum, as well as a measurable photoconductivity signal, extends all the way down to $\approx$2 eV[9] and, therefore, overlaps the entire blue side ($E > E_{max}$) of the absorption spectrum, it is not unreasonable to suspect that continuum states might play a role in the tail of the absorption spectrum. Although

this would explain the absence of a tail in previous one-electron simulations, this cannot be the whole story because the PEWP-2 model *does* recover a substantial blue tail.[43,44]

Figure 3a compares the TB and PEWP-2 results to the experimental absorption spectrum. We have discussed these data at length in previous work,[2,43,44,81] so we only briefly recapitulate here. The TB model does a reasonable job of reproducing the main Gaussian feature in the spectrum, although the peak absorption intensity is blue-shifted (relative to experiment) by about 0.3 eV. However, the Lorentzian tail is completely absent in the TB simulation. (A very modest blue tail does appear when nuclear quantum effects are included,[92] but even so the agreement with experiment in the high-energy region of the spectrum remains quite poor.)

A PEWP-2 spectrum that does *not* account for electronic reorganization of the solvent (i.e., for changes in the induced dipoles upon excitation of the wave function) is quite similar to the TB result; see refs 43 and 44. However, when electronic relaxation *is* taken into account, either perturbatively[43,44] or self-consistently,[81] we obtain spectra that are in much better agreement with experiment, as seen in Figure 3a. Electronic relaxation reduces the excited-state energies and thereby shifts the entire spectrum to the red and into better agreement with the experimental intensity maximum. At the same time, electronic relaxation modifies the transition dipoles, shifting oscillator strength from the lowest $s \rightarrow p$ transitions (which are the only bright states, within a "spherical box" model[2]) and into higher-lying bound states and quasi-continuum states, leading to the appearance of a blue tail.[43,44] Above 3.2 eV, however, the agreement with experiment remains rather poor and does not improve when more excited states are calculated (see Figure 3a). To some extent, this discrepancy may result from lifetime broadening effects that are not incorporated here (as discussed in section 4.3), but in any case the high-energy portion of the $e^-$(aq) spectrum deserves further study in future work.

Figure 3b plots the LGS and LGS-mPol spectra, including both Ewald and minimum-image versions of the former. The minimum-image LGS spectrum, which has been discussed previously,[46,47] is somewhat red-shifted, relative to experiment, but does exhibit a substantial blue tail. Larsen et al.[46] have noted that reasonable agreement with experiment is obtained by shifting this spectrum by ≈0.15 eV. However, the LGS/Ewald spectrum, which is reported here for the first time, requires a larger shift (≈ 0.4 eV) to bring the absorption maximum into agreement with experiment, and even the shifted spectrum is by no means clearly superior to the *unshifted* spectrum obtained from the PEWP-2 model following electronic relaxation (see Figure 3c). On the other hand, the shifted LGS/Ewald spectrum is in much better agreement with experiment than is the TB spectrum.

In an effort to resolve some of these ambiguities, we next turn to TD-DFT calculations.

## 4. RESULTS FROM TD-DFT

**4.1. Motivation.** In previous work, we have demonstrated that *many*-electron QM/MM calculations, where long-range-corrected TD-DFT is used to describe the QM region and where solvent configurations are sampled from the TB pseudopotential model, afford an optical spectrum that is in good agreement with experiment.[43] The agreement is quantitative for the main, Gaussian portion of the spectrum, and a long tail on the blue side of the spectrum is obtained as well. (The intensity of this tail is not in quantitative agreement with experiment, for reasons that are discussed in section 4.3.) Here, we report and analyze analogous TD-DFT/MM calculations, using geometries extracted from each of the simulations described above.

DFT and Hartree−Fock calculations suggest that, to rationalize certain properties of $e^-$(aq), one must accept that 10−20% of the aqueous electron's spin density is supported by frontier molecular orbitals centered on water molecules in the first solvation shell.[94−96] (Long ago, Kevan[97] estimated that 4% of the spin density must reside on first-shell water molecules to explain electron spin resonance data.) Furthermore, Bartels and co-workers[98] have recently reported a new measurement of the integrated oscillator strength (or "*f*-value") of the $e^-$(aq) absorption spectrum, for which they obtain a value of ≈1.1. According to the Thomas−Reiche−Kuhn (TRK) sum rule,[80,99] the sum of all oscillator strengths out of the ground state equals the number of electrons:

$$\sum_{n>0}^{\text{states}} f_{0\rightarrow n} = N_e \tag{8}$$

In view of eq 8, Bartels and co-workers[98] argue that their measurement implies that the spectrum *cannot* result from a strictly one-electron transition.

On the other hand, each of these results suggests a deviation from one-electron character of no more than 20%, and perhaps less, and it is not clear whether such an effect is *qualitatively* important. In this regard, we note that one-electron pseudopotential models neglect (at least) two effects: first, penetration of the unpaired electron into regions of space occupied by the valence MOs of the water molecules; and second, any possible many-electron character to the electronic excitations.

These two effects are not precisely equivalent, and TD-DFT in its standard form (i.e., linear-response theory within the adiabatic approximation) provides a framework in which they can be separated to some extent. Within a TD-DFT calculation, basis functions centered on the water molecules are available to the ground-state wave function of the electron (i.e., the SOMO), and virtual MOs on the water molecules are also available for the description of excited states. As such, both the ground and excited states of the excess electrons are free to delocalize into the MOs of the water molecules. In addition, TD-DFT calculations preserve the TRK sum rule in the complete-basis limit,[100,101] so the total oscillator strength within a TD-DFT calculation can certainly exceed unity.[103] However, *true* multiple excitations are absent in adiabatic, linear-response TD-DFT.[100,102]

**4.2. Computational Methods and Convergence Tests.** The description of $e^-$(aq) and $(H_2O)_n^-$ using DFT and TD-DFT is often problematic for at least two reasons. First, self-interaction error tends to overstabilize the anion relative to the underlying neutral solvent structure, which results in VEBEs that are ≳0.5 eV too large.[89] In addition, incorrect asymptotic behavior of the exchange−correlation potential results in severe underestimation of charge-transfer excitation energies in TD-DFT, with disastrous consequences in liquids and clusters.[104−106] However, recently developed long-range-corrected (LRC) density functionals, which asymptotically incorporated full Hartree−Fock (HF) exchange via a partitioned Coulomb operator, have been shown to mitigate both of these problems.[107−112]

All calculations reported here employ the LRC-$\mu$BOP functional,[113] which combines the so-called one-parameter progressive correlation functional[116] (OP) with a short-range version[117]

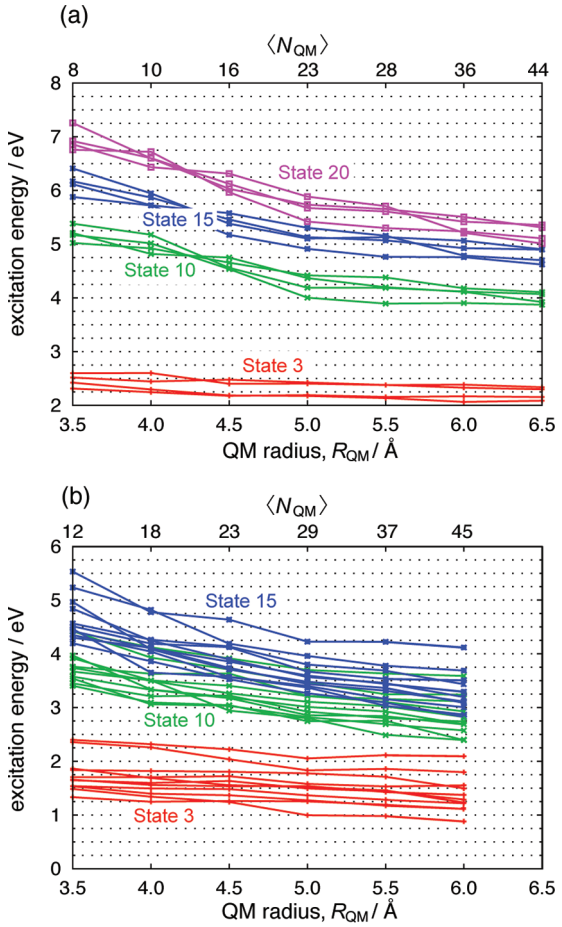


**Figure 4.** Convergence of TD-LRC-$\mu$BOP/6-31+G* excitation energies, as a function of the radius of the QM region, for (a) 4 different snapshots extracted from a bulk $e^-$(aq) simulation using the TB pseudopotential model, and (b) 11 different snapshots extracted from a simulation using the LGS model. The upper horizontal axis in either panel indicates the average number of water molecules in the QM region, $\langle N_{QM} \rangle$.

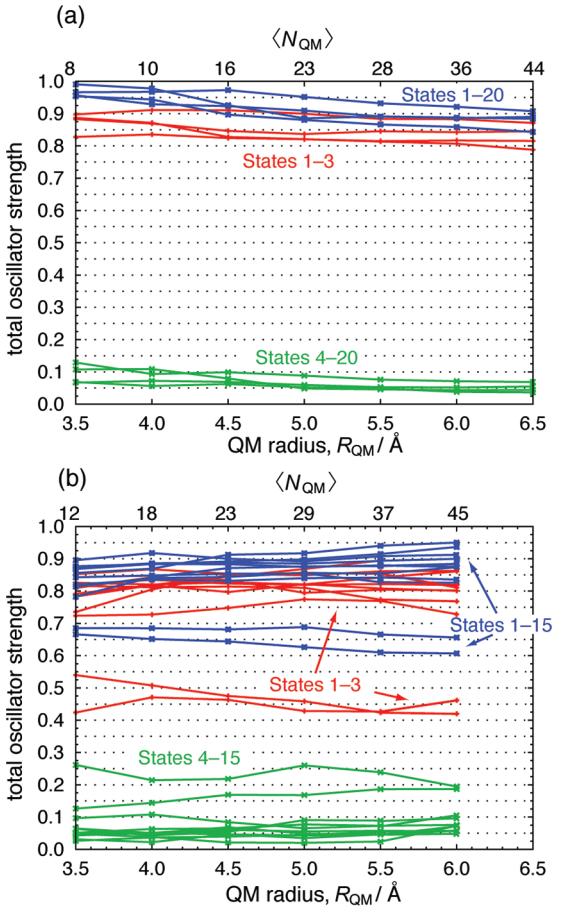


**Figure 5.** Convergence of the TD-LRC-$\mu$BOP/6-31+G* oscillator strengths as a function of the radius of the QM region for (a) snapshots extracted from the TB model of $e^-$(aq) and (b) snapshots extracted from the LGS model. The snapshots are the same as those used in Figure 4.

of Becke's generalized gradient exchange functional[118] ("$\mu$B88"), along with a long-range correction (LRC) consisting of 100% Hartree−Fock exchange. Altogether, the LRC-$\mu$BOP exchange-correlation energy expression is

$$E_{xc}^{\text{LRC-}\mu\text{BOP}} = E_c^{OP} + E_x^{\mu\text{B88, SR}} + E_x^{\text{HF, LR}} \quad (9)$$

The notation "SR" and "LR" indicates that only the short-range or long-range parts of the Coulomb operator are used to evaluate certain energy components. As in our previous work,[43] the Coulomb attenuation parameter is set to $\mu = 0.37\ a_0^{-1}$ in these calculations. For values of $\mu$ that are not too much different from this, the LRC-$\mu$BOP functional affords highly accurate VEBEs for $(H_2O)_n^-$ isomers.[66,90,119]

Here, we simulate the TD-DFT optical spectrum of $e^-$(aq) using solvent configurations extracted from various one-electron pseudopotential models. Starting from equilibrated trajectories for $e^-$(aq), obtained from the one-electron pseudopotential models as described in section 2.2, solvent configurations were extracted every 0.5 ps. The QM/MM partition was taken to be a sphere of radius $R_{QM}$ whose origin is the centroid of the one-electron wave function, and any $H_2O$ molecule with a

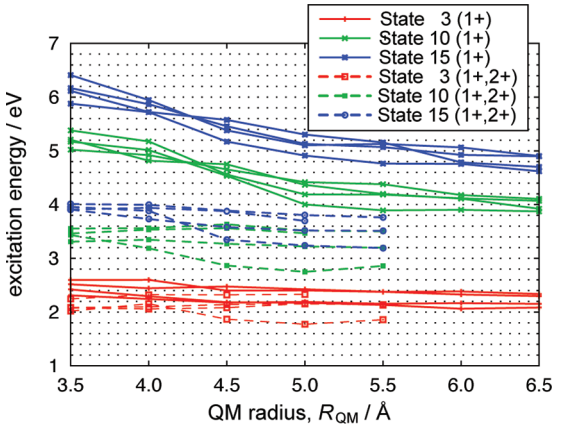


**Figure 6.** Convergence of the TD-LRC-$\mu$BOP excitation energies in the 6-31+G* [≡ 6-31(1+)G*] basis set, as compared to the convergence behavior, using the 6-31(1+,2+)G* basis set. Snapshots were extracted from the TB model of $e^-$(aq).

nucleus inside of this sphere was placed into the QM region. The MM region (represented by point charges $q_O = -0.82\ e$ and $q_H = +0.41\ e$) extends out to 50 Å, for a total of ~18000 water molecules. Such a large MM radius was chosen to ensure that the

diffuse MOs from the QM region do not penetrate beyond the MM region and into vacuum.

Figure 4 illustrates the convergence of the TD-DFT excitation energies, as a function of $R_{QM}$, for several different solvent configurations extracted from the TB and LGS pseudopotential models. In the TB case, we are able to extend these calculations out to $R_{QM}$ = 6.5 Å, at which point more than two full solvation shells around the cavity-bound electron are included in the QM region, and based on these tests we find that $R_{QM}$ = 5.5 Å is sufficient to converge the excitation energies to within 0.2−0.3 eV, at least for the lowest 15 excited states, and this value is used for all of the calculations reported in section 4.3. The LGS geometries include more water molecules at any particular value of $R_{QM}$, so we have extended these calculations only up to $R_{QM}$ = 6.0 Å; nevertheless, the convergence behavior is quite similar to that observed for the TB geometries. Convergence of the excitation energies is essentially monotonic from above as $R_{QM}$ is increased, which implies that a larger QM region ($R_{QM}$ > 5.5 Å) should red-shift the spectrum, but any such shift is likely to be quite small because the lowest three states, which carry the majority of the oscillator strength, are converged at $R_{QM}$ = 5.5 Å.

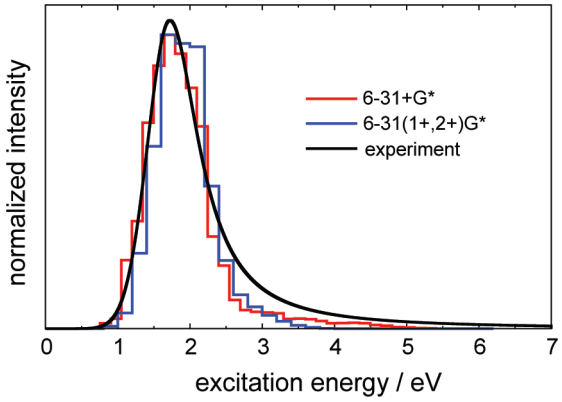


**Figure 7.** Comparison of TD-LRC-$\mu$BOP absorption spectra for $e^-$(aq) in bulk water, computed using two different basis sets. Geometries were extracted from a bulk simulation using the TB model, as described in the text.

Convergence of the oscillator strengths is examined in Figure 5. Despite some early indications that oscillator strengths might be quite sensitive to the size of the QM region,[2,43] a more careful analysis shows that the convergence is in fact quite rapid as a function of $R_{QM}$ if one considers the total oscillator strength for a group of states (e.g., the lowest three excited states, representing the $1s \rightarrow 1p$ excitations). The distribution of oscillator strengths obtained using LGS geometries is slightly different in that, on occasion, we observe that the *fourth* excited state sometimes exhibits significant oscillator strength; this is seen in 2 out of 11 snapshots depicted in Figure 5b. Despite this feature, the oscillator strengths do appear to be reasonably well converged for $R_{QM}$ = 5.5 Å, even in this case.

In every case, we note that the total oscillator strength supported by the lowest 15−20 excited states is less than unity. Furthermore, all of these states lie below 6.4 eV, which is much too low for $H_2O$ excitations; these do not appear until ∼8.0 eV at the TD-LRC-$\mu$BOP/6-31+G* level of theory. To the extent that

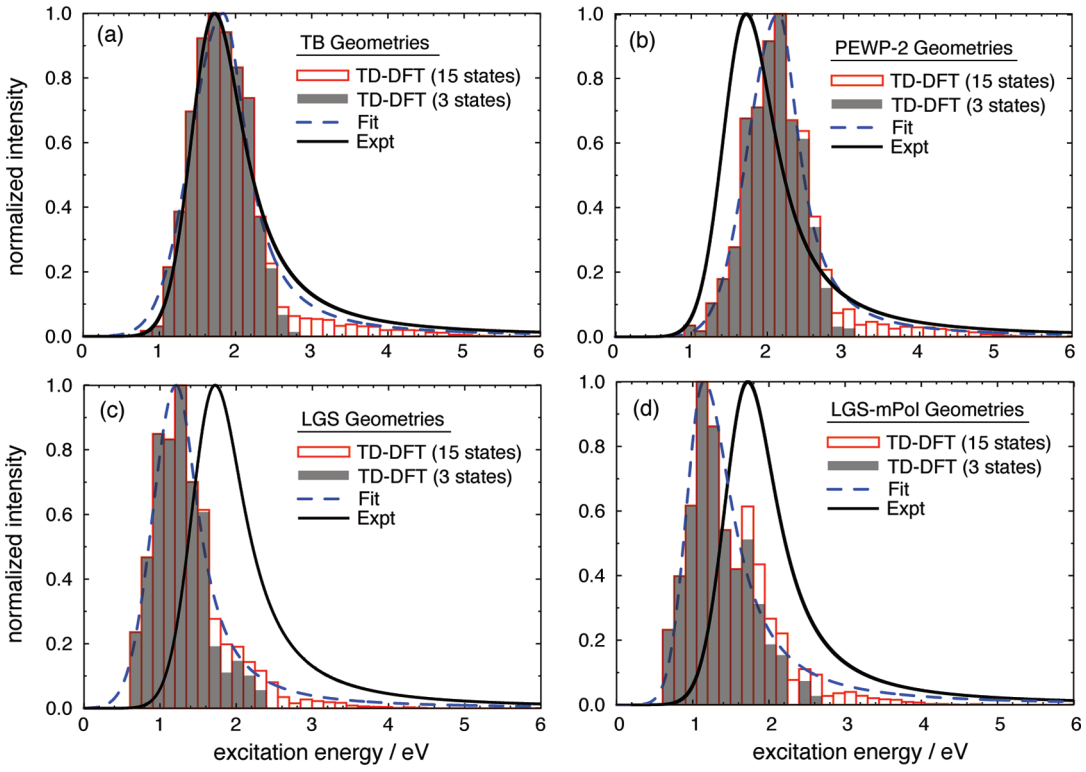


**Figure 8.** Histograms of TD-DFT excitation energies (weighted by oscillator strengths) averaged over solvent configurations obtained from various one-electron pseudopotential models. The shaded histograms represent the results of TD-DFT calculations in which only three excited states are included, whereas the open histograms result from the lowest 15 excited states. Ewald summation was employed in the TB and PEWP-2 simulations, whereas the LGS simulations used the minimum-image convention. Histogram bin widths are 0.15 eV, and fits of the histogram data to the line shape function in eq 7 are also shown.

**Table 2. Line Shape Parameters for the $e^-$(aq) Absorption Spectrum at $T$ = 298 K and Normal Water Density, Obtained from Fits to the TD-DFT Data**

| TD-DFT | | line shape parameters (eq 7)[a] | | | | |
|---|---|---|---|---|---|---|
| model | protocol | $E_{max}$/eV | $\sigma_G$/eV | $\sigma_L$/eV | FWHM/eV[b] | $\langle r_g \rangle$/Å[c] |
| TB | Ewald | 1.836 ± 0.026 | 0.419 ± 0.024 | 0.378 ± 0.028 | 1.121 | 2.50 |
| PEWP-2 | Ewald | 2.147 ± 0.022 | 0.395 ± 0.020 | 0.329 ± 0.024 | 1.030 | 2.30 |
| LGS | min. image | 1.211 ± 0.019 | 0.308 ± 0.018 | 0.361 ± 0.021 | 0.907 | 3.01 |
| LGS-mPol | min. image | 1.144 ± 0.034 | 0.227 ± 0.030 | 0.469 ± 0.040 | 0.872 | 2.85 |
| experiment[d] | | 1.721 | 0.304 | 0.495 | 1.034 | 2.40 |
| experiment[e] | | 1.735 | 0.304 | 0.483 | 1.022 | 2.40 |

[a] Uncertainties represent the asymptotic standard error in the nonlinear fit to the TD-DFT data. [b] Full width at half-maximum (FWHM) computed from the line shape function. [c] Radius of gyration computed from the line shape function. [d] Fit (from ref 9) to experimental data from ref 124. [e] Fit (from ref 9.) to experimental data from refs 125 and 126.

this is a reliable level of electronic structure theory, we can account for essentially all of the $e^-$(aq) oscillator strength via one-electron excitations of the unpaired electron.

We should point out that the 6-31+G* basis set used in these calculations would be wholly inadequate for studies of $(H_2O)_n^-$ clusters, where far more diffuse basis sets are required to describe weakly-bound cluster isomers in which the unpaired electron may penetrate significantly beyond the water network.[11,89] In the condensed phase, however, we anticipate that the SOMO is much more compact. In fact, the experimental value[9] $r_g$ = 2.44 Å for $e^-$(aq) at $T$ = 298 K is comparable to the full width at half-maximum (FWHM) of the diffuse functions in the 6-31+G* basis set (FWHM = 2.3 Å). This is larger than the typical distance between nearest-neighbor water molecules in the bulk liquid, so it would seem that the 6-31+G* basis functions cover the interstices in liquid water fairly well. Plots of the TD-DFT natural transition orbitals in ref 43 also demonstrate that the 6-31+G* basis set is capable of representing a cavity-centered SOMO.

On the other hand, excitation energies will become increasingly sensitive to the diffuseness of the basis set as one moves up the manifold of excited states. Figure 6 shows that, for $R_{QM}$ = 5.5 Å, the TD-LRC-$\mu$BOP/6-31+G* excitation energies for the first three excited states are essentially converged with respect to those computed using the more diffuse 6-31(1+,2+)G* basis set. However, for the higher-lying states that comprise the "blue tail" in the $e^-$(aq) absorption spectrum, the more diffuse basis set lowers the excitation energies by 1 eV or more.

To understand how this impacts the computed absorption spectrum, Figure 7 compares absorption spectra computed using these two basis sets. The resulting spectra are found to be quite similar. In particular, the peak absorption intensity and the width of the Gaussian feature are essentially the same in either spectrum, and in either case, a nontrivial tail is observed at higher excitation energies. This tail is somewhat attenuated in the more diffuse basis set because this basis lowers the energies of the higher-lying states (with respect to the more compact 6-31+G*) to a much greater extent for the higher-lying states than for the first few excited states. To obtain significant intensity above ~3.5 eV in the larger basis, we would need to compute a much larger number of excited states, which would make the calculations prohibitively expensive. Moreover, the *quantitative* differences between the blue tails obtained with either basis set are not large. For these reasons, and because we are somewhat wary of having basis functions that extend well into the MM region, as these might support artificial Rydberg excitations, all subsequent calculations employ the 6-31+G* basis set.

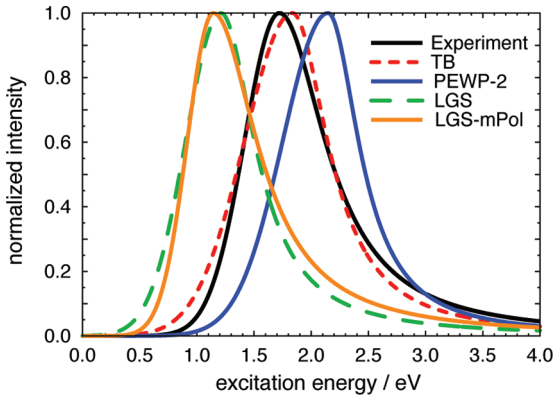


**Figure 9.** Line shape functions (eq 7) obtained as fits to the TD-DFT excitation energies and oscillator strengths.

All TD-DFT calculations were performed using Q-Chem, v. 3.2.[115] The Tamm-Dancoff approximation (TDA),[120] which is invoked by default in Q-Chem 3.2, is *not* used here, because the TRK sum rule for oscillator strengths, eq 8, is no longer strictly valid within the TDA. (However, a limited analysis of calculations performed within the TDA suggests that this approximation increases the $1s \rightarrow 1p$ excitation energies by ~0.1 eV relative to full linear response but has little other effect on the overall spectrum.) The SG-0 quadrature grid is used in all calculations, as we have shown this grid to be adequate for the sort of system and functional that is examined here.[89,121] Our choice of $R_{QM}$ = 5.5 Å leads to an average of 29 QM water molecules for snapshots extracted from the cavity-forming pseudopotential models and 37 QM water molecules for snapshots extracted from the LGS models.

**4.3. TD-DFT Spectra.** Figure 8 plots histograms of TD-DFT excitation energies for each pseudopotential model, in comparison to the experimental absorption spectrum. For the TB and PEWP-2 models, the histograms include 138 and 124 snapshots, respectively, but owing to the increased cost of the LGS calculations, as a result of the larger number of QM water molecules, only 60 snapshots are used in this case. (In addition, only LGS minimum-image geometries, and not LGS Ewald geometries, are used in the TD-DFT calculations.) For the PEWP-2 and TB data, we obtain essentially the same spectrum using only half of the data set, with an intensity maximum that shifts by less than the

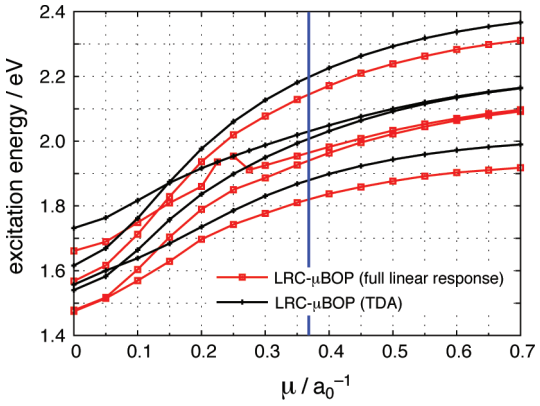


**Figure 10.** Dependence of the mean $1s \rightarrow 1p$ excitation energy, computed at the TD-LRC-$\mu$BOP/6-31+G* level, on the Coulomb attenuation parameter, $\mu$. Results are shown for four different QM/MM snapshots taken from the TB model. (These are the same four snapshots used in Figures 4a and 5a.) In each case, what is plotted is the weighted average (according to oscillator strength) of the three lowest TD-DFT excitation energies. Results are shown for both the Tamm−Dancoff approximation (TDA) as well as full linear response theory, although only the latter approach is used to compute spectra. The solid vertical line denotes the value of $\mu$ used to compute spectra in this work.

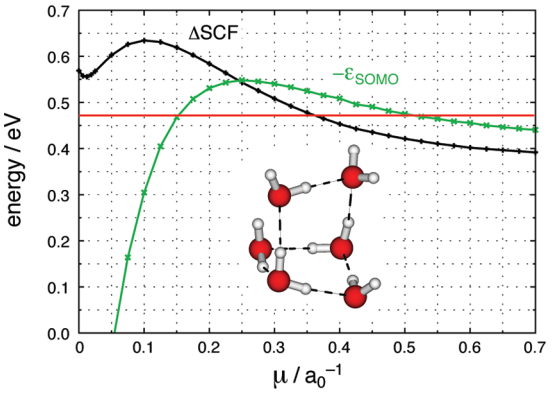


**Figure 11.** VEBE of the "OP1-AA" isomer[130] of $(H_2O)_6^-$, computed at the LRC-$\mu$BOP level and plotted as a function of the Coulomb attenuation parameter, $\mu$. The calculation was performed in two ways: first, by means of the usual $\Delta$SCF procedure [VEBE = $E$(neutral) − $E$(anion)]; and second, using the SCF eigenvalue for the SOMO (VEBE = $-\varepsilon_{SOMO}$). The solid horizontal line represents the VEBE obtained from a large-basis CCSD(T) calculation.[131] DFT calculations used the "aug-cc-pVDZ+diff" basis recommended by Yagi et al.[90].

width of one histogram bin (<0.15 eV). Therefore, while we expect that more snapshots for the LGS model would smooth out some of the fluctuations in the histograms (e.g., around 1.1 eV in Figure 8c and around 1.5 eV in Figure 8d), we also suspect that fits of these histograms to the line shape function are probably nearly converged with respect to sampling. Furthermore, the rapid convergence of the $1s \rightarrow 1p$ excitation energies suggests that the absorption maximum is well converged in all cases.

Fits of the TD-DFT histogram data to the line shape function in eq 7 are also shown in Figure 8, and best-fit parameters are reported in Table 2. These analytic line shape functions can be used to determine the radius of gyration corresponding to each TD-DFT line shape. Expressed in atomic units, the relation between $\langle r_g \rangle$ and $I(E)$ is[9,122,123]

$$\langle r_g \rangle = \left[ \frac{3\int_0^\infty E^{-1} I(E)\mathrm{d}E}{2\int_0^\infty I(E)\mathrm{d}E} \right]^{1/2} \quad (10)$$

Values of $\langle r_g \rangle$ determined from the TD-DFT spectra are reported in Table 2 and should be compared to the values determined directly from the one-electron pseudopotential simulations, using the definition in eq 6. The latter are reported in Table 1.

As we have reported previously,[43] the spectrum computed from TB geometries (Figure 8a) is in essentially *quantitative* agreement with the experimental spectrum once the TD-DFT data are fit to the line shape function in eq 7. In addition, the radius of gyration determined from the TD-DFT line shape ($\langle r_g \rangle$ = 2.50 Å) agrees well with the value that is determined directly from the TB model's ground-state wave function ($\langle r_g \rangle$ = 2.45 Å).

Looking carefully at the histogram of excitation energies in Figure 8a, rather than the fitted line shape, one could reasonably argue that, although the low-energy, Gaussian portion of the histogram *is* in quantitative agreement with experiment, the blue tail is not. Two sources of error likely contribute to this diminished intensity in the simulated blue tail. One is the rather compact basis set that is employed in the TD-DFT calculations, whereas the states that comprise the blue tail are quite diffuse.[2,43,44] As noted above, additional diffuse functions significantly lower the higher-lying excitation energies, which suggests that, for a more quantitative representation of the blue tail, we should use a more diffuse basis set and also calculate far more excited states. A second source of error is intrinsic to the use of the heterogeneous broadening formula in eq 5 to calculate the spectral intensity, which neglects the effects of lifetime broadening. We have previously suggested[2,44] that lifetime broadening may be important, given the relatively high density of states in the blue tail. This suggestion is supported by the observation[9] that the optical spectra of $e^-$(aq) in both $H_2O$ and $D_2O$ can be fit using the same $\sigma_G$ parameter, whereas $\sigma_L^{D_2O} \approx 0.906\ \sigma_L^{H_2O}$. As pointed out by Coe et al.,[9] this observation suggests that dynamics play some role in determining $\sigma_L$.

Despite these shortcomings, the agreement between the experimental spectrum and the TD-DFT spectrum computed from TB geometries is striking. In comparison, TD-DFT spectra based on geometries extracted from the other pseudopotential models are in less good agreement with experiment. Geometries from our model, PEWP-2, lead to a spectrum that is blue-shifted by about 0.4 eV relative to experiment and by 0.3 eV relative to the spectrum based on TB geometries. This can be rationalized in terms of a radius of gyration that is ≈0.2 Å too small (whether computed using the PEWP-2 wave function or the TD-DFT line shape obtained from PEWP-2 geometries). A reduction in the cavity size, and hence, $r_g$, should result in a blue shift of the $1s \rightarrow 1p$ excitation energies. The magnitude of this shift can be understood in terms of a "spherical box" model using parameters (cavity size and binding energy) that roughly reproduce the experimental radius of gyration, the $1s \rightarrow 1p$ excitation energy, and the VEBE.[2] Within such a model, a reduction in the radius of the box that is sufficient to reduce $r_g$ by 0.2 Å also affords a 0.3 eV blue shift in the $1s \rightarrow 1p$ excitation energy.

The LGS and LGS-mPol geometries, in contrast, produce TD-DFT spectra that are red-shifted by 0.5−0.6 eV relative to experiment. Moreover, the radii of gyration that are extracted from the TD-DFT line shapes are inconsistent with the values

computed directly from the ground-state one-electron wave functions. In the case of the LGS/Ewald simulations, for example, these two methods afford $r_g$ = 2.69 Å (from the one-electron wave function) and $r_g$ = 3.01 Å (from the TD-DFT line shape).

The line shape functions obtained by fitting the TD-DFT histogram data are plotted together in Figure 9. It is interesting to note that the TD-DFT spectra obtained using LGS and LGS-mPol geometries are extremely similar to one another, despite the fact that LGS-mPol significantly reduces the magnitude of the polarization potential.[91] This indicates that solvent geometries do not differ greatly between these two models, which implies that it is the LGS pseudopotential itself, and not the details of the ad hoc polarization potential, that is responsible for the non-cavity-forming nature of the model and for the substantially red-shifted spectra computed from TD-DFT.

In evaluating these TD-DFT spectra, it is worth recalling the essentially monotonic convergence of TD-DFT excitation energies as a function of $R_{QM}$ (Figure 4), which implies that a larger QM region would only shift the spectra further to the red. (However, we do not expect this shift to be large because the first three excitation energies, which carry most of the oscillator strength, are essentially converged for the value $R_{QM}$ = 5.5 Å that is used here.) Moreover, judging from the FWHM data reported in Table 2, the TD-DFT line shape functions obtained from LGS and LGS-mPol geometries are too narrow, by a bit more than 0.1 eV, whereas the TD-DFT spectrum obtained from TB geometries is too wide, by about the same amount. As with the red-shifts in the LGS spectra, a larger QM region will not alleviate this problem because the convergence tests in section 4.2 indicate that the width of the Gaussian feature is probably converged already and, therefore, the effect of lowering the higher-lying excitation energies (by increasing the size of the QM region or the diffuseness of the basis set) will be to reduce the FWHM of the simulated spectrum. This correction is likely to be small because the first few excited states appear to be well converged.

**4.4. Assessment of LRC-$\mu$BOP.** The quality of our TD-DFT calculations is potentially subject to criticism, which we address here. Although the LRC-$\mu$BOP functional with $\mu$ = 0.33 $a_0^{-1}$ has been shown to afford very accurate VEBEs for $(H_2O)_n^-$ clusters,[66,90] the Coulomb attenuation parameter, $\mu$, is probably the most ambiguous and least theoretically justified parameter in this particular density functional. Benchmark tests on a wide range of systems indicate that both ground-state properties as well as TD-DFT excitation energies can be quite sensitive to the value of $\mu$.[111,121]

In Figure 10, we illustrate the $\mu$-dependence of the mean $1s \rightarrow 1p$ excitation energy, that is, the weighted average (according to oscillator strength) of the three lowest excitation energies, which is a proxy for the absorption maximum. We observe that this mean value shifts to higher energy as $\mu$ increases, which is consistent with an overall trend toward higher excitation energies in TD-LRC-DFT, as a function of $\mu$, for excited states that do not exhibit significant charge-transfer character.[111] In this context, we recall that TD-DFT spectra based on LGS and LGS-mPol geometries are red-shifted by at least 0.5 eV, and the $\mu$-dependence documented in Figure 10 demonstrates that it would be essentially impossible to induce anything approaching a 0.5 eV blue shift simply by changing the value of $\mu$. (Note also that LRC functionals engender significant errors for $\mu \gtrsim 0.9\ a_0^{-1}$,[111,121] and benchmark studies have consistently recommended values of $\mu < 0.5\ a_0^{-1}$,[108,109,111,117,121,127] so any push toward larger $\mu$ to increase the excitation energies is inadvisible on general theoretical grounds.)

We have also computed TD-DFT excitation energies using the BLYP and B3LYP functionals[118,128,129] for the four snapshots used in Figure 10. We find that the $1s \rightarrow 1p$ excitation energies obtained from TD-BLYP and TD-B3LYP calculations are quite close to the values obtained from TD-LRC-$\mu$BOP, with $\mu = 0$ and $\mu = 0.1\ a_0^{-1}$, respectively. This makes sense, given that the $\mu \rightarrow 0$ limit of LRC-$\mu$BOP affords the BOP functional, which is a reparameterized version of BLYP,[116] and given that TD-B3LYP excitation energies are generally somewhat higher than TD-BLYP results owing to the 20% Hartree−Fock exchange present in B3LYP. In any case, these results demonstrate that appealing to more widely-used functionals such as BLYP and B3LYP would only move the spectrum computed from LGS geometries further away from the experimental result.

Baer and co-workers[112] recommend tuning $\mu$ in a system-specific fashion, and one suggested criterion for doing so is to insist that the negative eigenvalue, $-\varepsilon_{HOMO}$, of the highest occupied Kohn−Sham MO (HOMO) should equal the ionization potential of the molecule. This condition is satisfied by the exact Hohenberg−Kohn density functional but is poorly approximated by most contemporary density-functional approximations, with the exception of certain LRC functionals. To evaluate this ionization potential criterion here, we choose a certain isomer of $(H_2O)_6^-$ whose ionization potential (i.e., VEBE) has been calculated at numerous levels of theory by Jordan and co-workers.[130,131] As a benchmark VEBE for this cluster isomer, we take the large-basis CCSD(T) value reported in ref 131, which lies within the statistical error bars of quantum Monte Carlo results for the same isomer.[131]

Figure 11 compares the CCSD(T) benchmark to a LRC-$\mu$BOP calculation of the VEBE, as a function of $\mu$. As expected,[90] the LRC-$\mu$BOP result lies very close to the benchmark for $\mu \approx 0.33\ a_0^{-1}$. Also shown in Figure 11 is the $\mu$-dependent value of $-\varepsilon_{SOMO}$. Exact agreement between $-\varepsilon_{SOMO}$ and the benchmark VEBE is achieved for a rather small value of the Coulomb attenuation parameter, $\mu = 0.15\ a_0^{-1}$, however, the "ΔSCF" result [i.e., the VEBE calculated based on separate DFT calculations of $(H_2O)_n$ and $(H_2O)_n^-$] is in reasonable agreement with $-\varepsilon_{SOMO}$ for the value $\mu = 0.37\ a_0^{-1}$ that is used in this study. In any case, these data fail to justify any large increase in $\mu$ that might shift the LGS spectra substantially to the blue and thus into better agreement with experiment.

## 5. SUMMARY AND CONCLUSIONS

The recently proposed Larsen−Glover−Schwartz (LGS) one-electron pseudopotential model for the hydrated electron,[46] in which the unpaired electron does not localize into a well-defined solvent cavity, has been evaluated here in comparison to two other one-electron models that do predict such a cavity.[41,44] While comparisons of the LGS model against experimental data for $e^-$(aq) have been reported previously,[46,47,52] the present work represents the first time that Ewald summation (rather than the minimum-image convention) has been used in the context of the LGS model. We find that certain observables such as the electron's radius of gyration ($r_g$) and optical absorption spectrum, which the LGS model had been thought to reproduce reasonably well,[46] are in less favorable agreement with experiment when Ewald summation is employed. A substantial error in the LGS value of the vertical electron binding energy (VEBE) for $e^-$(aq), which had been

reported previously,[47] is further exacerbated by the use of Ewald summation, so that the bulk VEBE predicted by the LGS model is 1−2 eV higher than any experimental estimate of this quantity. In contrast, reasonable values of $r_g$ are obtained from the cavity-forming models, and the bulk VEBE and optical absorption maximum are in good agreement with experiment, when corrected for the effects of electronic reorganization of the solvent.

In addition to these experimental comparisons, we have used TD-DFT calculations, in conjunction with a carefully calibrated QM/MM protocol, in an effort to assess various structural motifs for $e^-$(aq). TD-DFT calculations using solvent configurations extracted from the cavity-forming TB model are in nearly quantitative agreement with the experimental absorption line shape, save for a slightly diminished intensity in the high-energy tail that likely results from inadequacies in the present TD-DFT treatment. When solvent configurations are taken instead from the cavity-forming PEWP-2 model, the resulting TD-DFT spectrum is somewhat blue-shifted relative to experiment, consistent with a PEWP-2 radius of gyration that is slightly smaller than the value derived from the experimental absorption line shape. On the other hand, the TD-DFT spectrum based on noncavity LGS geometries is severely red-shifted relative to experiment. We have explored a variety of modifications to both the QM/MM protocol and the DFT functional, but each of these changes appears to exacerbate the discrepancy between the LGS spectrum and experiment.

Given that the LGS model predicts a radius of gyration, electronic absorption spectrum, and VEBE that are markedly different from the corresponding experimental data, it is reasonable to ask what data are left that might lend credence to this model of $e^-$(aq). For one, the calculated value of the $e^-$(aq) diffusion constant at $T$ = 300 K, using the LGS model, has been found to be within a factor of 2 of the experimental value,[46] although it is noteworthy that the LGS value is too small by a factor of 2, whereas $H_2O$ self-diffusion is too *fast*, again by about a factor of 2, for the underlying SPC water model.[132] The LGS model also rationalizes the absence of any polarization-dependent bleaching dynamics in transient hole-burning experiments,[46] whereas older cavity-forming models predicted that such dynamics should be observable.[133,134] However, recent theoretical work suggests that ultrafast depolarization of the $1s \rightarrow 1p$ transition dipoles may explain the absence of an experimental signal, even in the context of a cavity-bound electron.[44,53] Finally, previous claims[52,56] that the LGS model might explain the negative partial molar volume of $e^-$(aq) have been shown to result from a misinterpretation of the experimental literature.[54] These observations leave precious little to support the noncavity interpretation of $e^-$(aq).

This work is unlikely to be the final word regarding the structure of $e^-$(aq). At present, however, it appears that the cavity-forming models of $e^-$(aq) offer the most consistent description of this species and the most accurate comparison to experimental data, at least within the framework of models based upon a one-electron, charge-defect description of $e^-$(aq).

## AUTHOR INFORMATION

### Corresponding Author

*E-mail: herbert@chemistry.ohio-state.edu.

### Present Addresses

[†]Dept. of Chemistry, Yale University, New Haven, CT.

## ACKNOWLEDGMENT

This work was supported by a National Science Foundation CAREER award (CHE-0748448) and calculations were performed at the Ohio Supercomputer Center under Project PAS0291. J.M.H. is an Alfred P. Sloan Foundation Fellow and a Camille Dreyfus Teacher-Scholar. L.D.J. acknowledges a Presidential Fellowship from The Ohio State University. Thomas Sommerfeld kindly provided the geometry for the OP1-AA isomer of $(H_2O)_6^-$, from ref 130.

## REFERENCES

(1) Mostafavi, M.; Lampre, I. In *Radiation Chemistry*; Spotheim-Maurizot, M., Mostafavi, M., Belloni, J., Douki, T., Eds.; EDP Sciences: U.K., 2008; Chapter 3, pp 33−52.
(2) Herbert, J. M.; Jacobson, L. D. *Int. Rev. Phys. Chem.* **2011**, *30*, 1–48.
(3) Siefermann, K. R.; Abel, B. *Angew. Chem., Int. Ed.* **2011**, *50*, 5264–5272.
(4) Hart, E. J.; Boag, J. W. *J. Am. Chem. Soc.* **1962**, *84*, 4090–4095.
(5) Boag, J. W.; Hart, E. J. *Nature* **1963**, *197*, 45–47.
(6) Buxton, G. V. In *Radiation Chemistry*; Spotheim-Maurizot, M., Mostafavi, M., Belloni, J., Douki, T., Eds.; EDP Sciences: U.K., 2008; Chapter 1, pp 3−16.
(7) Jordan, K. D.; Wang, F. *Annu. Rev. Phys. Chem.* **2003**, *54*, 367–396.
(8) Verlet, J. R. R.; Bragg, A. E.; Kammrath, A.; Cheshnovsky, O.; Neumark, D. M. *Science* **2005**, *307*, 93–96.
(9) Coe, J. V.; Williams, S. M.; Bowen, K. H. *Int. Rev. Phys. Chem.* **2008**, *27*, 27–51.
(10) Sommerfeld, T.; DeFusco, A.; Jordan, K. D. *J. Phys. Chem. A* **2008**, *112*, 11021–11035.
(11) Williams, C. F.; Herbert, J. M. *J. Phys. Chem. A* **2008**, *112*, 6171–6178.
(12) Robinson, G. W.; Thistlewaite, P. J.; Lee, J. *J. Phys. Chem.* **1986**, *90*, 4224–4233.
(13) Hameka, H. F.; Robinson, G. W.; Marsden, C. J. *J. Phys. Chem.* **1987**, *91*, 3150–3157.
(14) Sobolewski, A. L.; Domcke, W. *Phys. Chem. Chem. Phys.* **2002**, *4*, 4–10.
(15) Sobolewski, A. L.; Domcke, W. *J. Phys. Chem. A* **2002**, *106*, 4158–4167.
(16) Neumann, S.; Eisfeld, W.; Sobolewski, A.; Domcke, W. *Phys. Chem. Chem. Phys.* **2004**, *6*, 5297–5303.
(17) Sobolewski, A. L.; Domcke, W. *Phys. Chem. Chem. Phys.* **2007**, *9*, 3818–3829.
(18) Uhlig, F.; Marsalek, O.; Jungwirth, P. *Phys. Chem. Chem. Phys.* **2011**, *13*, 14003–14009.
(19) Tuttle, T. R., Jr.; Golden, S.; Lwenje, S.; Stupak, C. M. *J. Phys. Chem.* **1984**, *88*, 3811–3818.
(20) Tuttle, T. R., Jr.; Golden, S. *J. Phys. Chem.* **1991**, *95*, 5725–5736.
(21) Tauber, M. J.; Mathies, R. A. *J. Am. Chem. Soc.* **2003**, *125*, 1394–1402.
(22) Jortner, J.; Rice, S. A. Solvated Electron. In *Advances in Chemistry*; Gould, R. F., Ed.,American Chemical Society Publications: Washington, D.C., 1965; Vol. 50, Chapter 2, pp 7−26.
(23) Copeland, D. A.; Kestner, N. R.; Jortner, J. *J. Chem. Phys.* **1970**, *53*, 1189–1216.
(24) Gaathon, A.; Czapski, G.; Jortner, J. *J. Chem. Phys.* **1973**, *58*, 2648–2650.
(25) Parrinello, M.; Rahman, A. *J. Chem. Phys.* **1984**, *80*, 860–867.
(26) Sprik, M.; Imprey, R. W.; Klein, M. L. *J. Chem. Phys.* **1985**, *83*, 5802–5809.
(27) Sprik, M.; Impey, R. W.; Klein, M. L. *J. Stat. Phys.* **1986**, *43*, 967–972.
(28) Sprik, M.; Klein, M. L. *Comput. Phys. Rep.* **1988**, *7*, 147–166.

(29) Jonah, C. D.; Romero, C.; Rahman, A. *Chem. Phys. Lett.* **1986**, *123*, 209–214.
(30) Thirumalai, D.; Wallqvist, A.; Berne, B. J. *J. Stat. Phys.* **1986**, *43*, 973–984.
(31) Wallqvist, A.; Thirumalai, D.; Berne, B. J. *J. Chem. Phys.* **1986**, *85*, 1583–1591.
(32) Wallqvist, A.; Thirumalai, D.; Berne, B. J. *J. Chem. Phys.* **1987**, *86*, 6404–6418.
(33) Wallqvist, A.; Martyna, G.; Berne, B. J. *J. Phys. Chem.* **1988**, *92*, 1721–1730.
(34) Schnitker, J.; Rossky, P. J. *J. Chem. Phys.* **1987**, *86*, 3471–3485.
(35) Rossky, P. J.; Schnitker, J.; Kuharski, R. A. *J. Stat. Phys.* **1986**, *43*, 949–965.
(36) Schnitker, J.; Motakabbir, K.; Rossky, P. J.; Friesner, R. A. *Phys. Rev. Lett.* **1988**, *60*, 456–459.
(37) Rossky, P. J.; Schnitker, J. *J. Phys. Chem.* **1988**, *92*, 4277–4285.
(38) Schnitker, J.; Rossky, P. J. *J. Phys. Chem.* **1989**, *93*, 6965–6969.
(39) Park, I.; Cho, K.; Lee, S.; Kim, K. S.; Joannopoulos, J. D. *Comput. Mater. Sci.* **2001**, *21*, 291–300.
(40) Skorobogatiy, M.; Park, I. J.; Joannopoulos, J. D. *Comput. Mater. Sci.* **2005**, *32*, 96–106.
(41) Turi, L.; Borgis, D. *J. Chem. Phys.* **2002**, *117*, 6186–6195.
(42) Tay, K. A.; Boutin, A. *J. Phys. Chem. B* **2009**, *113*, 11943–11949.
(43) Jacobson, L. D.; Herbert, J. M. *J. Am. Chem. Soc.* **2010**, *132*, 10000–10002.
(44) Jacobson, L. D.; Herbert, J. M. *J. Chem. Phys.* **2010**, *133*, 154106:1–19.
(45) Boero, M.; Parrinello, M.; Terakura, K.; Ikeshoji, T.; Liew, C. C. *Phys. Rev. Lett.* **2003**, *90*, 226403:1–4.
(46) Larsen, R. E.; Glover, W. J.; Schwartz, B. J. *Science* **2010**, *329*, 65–69.
(47) Jacobson, L. D.; Herbert, J. M. *Science* **2011**, *331*, 1387.
(48) Madarasz, A.; Rossky, P. J.; Turi, L. *J. Phys. Chem. A* **2010**, *114*, 2331–2337.
(49) Marsalek, O.; Uhlig, F.; Frigato, T.; Schmidt, B.; Jungwirth, P. *Phys. Rev. Lett.* **2010**, *105*, 043002:1–4.
(50) Marsalek, O.; Uhlig, F.; Jungwirth, P. *J. Phys. Chem. C* **2010**, *114*, 20489–20495.
(51) Jacobson, L. D.; Herbert, J. M. *J. Am. Chem. Soc.* **2011**, DOI: 10.1021/ja208024p.
(52) Larsen, R. E.; Glover, W. J.; Schwartz, B. J. *Science* **2011**, *331*, 1387.
(53) Shkrob, I. A. *Chem. Phys. Lett.* **2008**, *467*, 84–87.
(54) In ref 52, LGS hypothesize that enhanced liquid density near the centroid of the $e^-$ wave function, which is a unique feature of their pseudopotential model, might explain why the partial molar volume of $e^-$(aq), $\overline{V}_e$, is negative. Reference 55 is cited by LGS as experimental evidence that $\overline{V}_e < 0$, a claim that has since been repeated elsewhere.[56] It is therefore worth noting that, in ref 55, Hentz et al. actually conclude only that $\overline{V}_e$ lies in the range from − 1.7 to + 2.7 mL/mol, that is, the experimental data are inconclusive as to the sign of $\overline{V}_e$. In fact, based on an estimate of the effects of electrostriction, Hentz et al.[55] argue that their data are consistent with an electron that occupies a cavity whose volume is 1−6 mL/mol, corresponding to a spherical cavity radius of 0.73−1.3 Å per electron, in reasonable agreement with existing cavity models of $e^-(aq)$. (See, for example, the RDFs in Figure 2.) Despite earlier experiments (from the same laboratory) indicating that $\overline{V}_e < 0$,[57,58] later measurements by Hentz et al. yielded values of $\overline{V}_e = 0$,[59] $\overline{V}_e =$ 0−13 mL/mol,[60] and $\overline{V}_e = +7$ mL/mol,[61] corresponding to cavity radii of 1.1 Å, 1.1−1.9 Å, and 1.6 Å, respectively,[61] assuming a spherical cavity and an electrostriction contribution of 3 mL/mol.[57] More recently, a cavity volume of 26 mL/mol, corresponding to a spherical cavity radius of 2.2 Å, has been measured by a completely different technique.[62,63]
(55) Hentz, R. R.; Brazier, D. W. *J. Chem. Phys.* **1971**, *54*, 2777–2780.
(56) Ben-Amotz, D. *J. Phys. Chem. Lett.* **2011**, *2*, 1216–1222.
(57) Hentz, R. R.; Farhataziz; Milner, D. J.; Burton, M. *J. Chem. Phys.* **1967**, *47*, 374–377.
(58) Hentz, R. R.; Farhataziz; Milner, D. J. *J. Chem. Phys.* **1967**, *47*, 5381–5383.
(59) Hentz, R. R.; Farhataziz; Hansen, E. M. *J. Chem. Phys.* **1972**, *56*, 4485–4488.
(60) Hentz, R. R.; Knight, R. J. *J. Chem. Phys.* **1970**, *52*, 2456–2459.
(61) Hentz, R. R.; Farhataziz; Hansen, E. M. *J. Chem. Phys.* **1972**, *57*, 2959–2963.
(62) Borsarelli, C. D.; Bertolotti, S. G.; Previtali, C. M. *Photochem. Photobiol. Sci.* **2003**, *2*, 791–795.
(63) Borsarelli, C. D. *J. Phys. IV* **2005**, *125*, 11–13.
(64) Turi, L.; Madarász, Á. *Science* **2011**, *331*, 1387.
(65) Toukan, K.; Rahman, A. *Phys. Rev. B* **1985**, *31*, 2643–2648.
(66) Jacobson, L. D.; Williams, C. F.; Herbert, J. M. *J. Chem. Phys.* **2009**, *130*, 124115:1–18.
(67) Schnitker, J.; Rossky, P. J. *J. Chem. Phys.* **1987**, *86*, 3462–3470.
(68) Barnett, R. N.; Landman, U.; Cleveland, C. L.; Jortner, J. *J. Chem. Phys.* **1988**, *88*, 4421–4428.
(69) Turi, L.; Sheu, W.-S.; Rossky, P. J. *Science* **2005**, *309*, 914–917.
(70) Turi, L.; Madarász, Á.; Rossky, P. J. *J. Chem. Phys.* **2006**, *125*, 014308:1–7.
(71) Borgis, D.; Rossky, P. J.; Turi, L. *J. Chem. Phys.* **2006**, *125*, 064501:1–13.
(72) Borgis, D.; Rossky, P. J.; Turi, L. *J. Chem. Phys.* **2007**, *127*, 174508:1–6.
(73) Madarász, Á.; Rossky, P. J.; Turi, L. *J. Chem. Phys.* **2007**, *126*, 234707:1–11.
(74) Madarasz, A.; Rossky, P. J.; Turi, L. *J. Chem. Phys.* **2009**, *130*, 124319:1–7.
(75) Takayanagi, T.; Yoshikawa, T.; Motegi, H.; Shiga, M. *Chem. Phys. Lett.* **2009**, *482*, 195–200.
(76) Ren, P.; Ponder, J. W. *J. Phys. Chem. B* **2003**, *107*, 5933–5947.
(77) Ren, P.; Ponder, J. W. *J. Phys. Chem. B* **2004**, *108*, 13427–13437.
(78) Thole, B. *Chem. Phys.* **1981**, *59*, 341–350.
(79) Cavanagh, M. C.; Martini, I. B.; Schwartz, B. J. *Chem. Phys. Lett.* **2004**, *396*, 359–366.
(80) McHale, J. L. *Molecular Spectroscopy*; Prentice Hall: New York, 1999.
(81) Jacobson, L. D.; Herbert, J. M. *J. Chem. Theory Comput.* **2011**, *7*, 2085–2093.
(82) Tang, Y.; Shen, H.; Sekiguchi, K.; Kurahashi, N.; Mizuno, T.; Suzuki, Y. I.; Suzuki, T. *Phys. Chem. Chem. Phys.* **2010**, *12*, 3653–3655.
(83) Siefermann, K. R.; Liu, Y.; Lugovoy, E.; Link, O.; Faubel, M.; Buck, U.; Winter, B.; Abel, B. *Nat. Chem.* **2010**, *2*, 274–279.
(84) Shreve, A. T.; Yen, T. A.; Neumark, D. M. *Chem. Phys. Lett.* **2010**, *493*, 216–219.
(85) Lübcke, A.; Buchner, F.; Heine, N.; Hertel, I. V.; Schultz, T. *Phys. Chem. Chem. Phys.* **2010**, *12*, 14629–14634.
(86) Ma, L.; Majer, K.; Chirot, F.; von Issendorff, B. *J. Chem. Phys.* **2009**, *131*, 144303:1–6.
(87) Makov, G.; Nitzan, A. *J. Phys. Chem.* **1994**, *98*, 3459–3466.
(88) For the database of $(H_2O)_n^-$ VEBEs ($2 \le n \le 33$) that we reported in ref 11, and which we believe to be accurate to within ≈ 0.05 eV in most cases,[11,66,89,90] the TB model exhibits a mean unsigned error of 0.253 eV (vs 0.209 eV for the LGS-mPol model) and a maximum absolute deviation of −0.746 eV (vs +0.689 eV for the LGS-mPol model), for VEBEs that range from ≈0 up to 2.5 eV.
(89) Herbert, J. M.; Head-Gordon, M. *J. Phys. Chem. A* **2005**, *109*, 5217–5229.
(90) Yagi, K.; Okano, Y.; Sato, T.; Kawashima, Y.; Tsuneda, T.; Hirao, K. *J. Phys. Chem. A* **2008**, *112*, 9845–9853.
(91) As pointed out in ref 52, the LGS-mPol model dramatically reduces the magnitude of $V_{pol}$, as compared to the original LGS polarization potential.
(92) Turi, L.; Hantal, G.; Rossky, P. J.; Borgis, D. *J. Chem. Phys.* **2009**, *131*, 024119:1–19.
(93) Coe, J. V. *Int. Rev. Phys. Chem.* **2001**, *20*, 33–58.
(94) Shiraishi, H.; Ishigure, K.; Morokuma, K. *J. Chem. Phys.* **1988**, *88*, 4637–4649.

(95) Shkrob, I. A. *J. Phys. Chem. A* **2007**, *111*, 5223–5231.
(96) Herbert, J. M.; Head-Gordon, M. *J. Am. Chem. Soc.* **2006**, *128*, 13932–13939.
(97) Kevan, L. *Acc. Chem. Res.* **1981**, *14*, 138–145.
(98) Hare, P. M.; Price, E. A.; Stanisky, C. M.; Janik, I.; Bartels, D. M. *J. Phys. Chem. A* **2010**, *114*, 1766–1775.
(99) Fano, U.; Cooper, J. W. *Rev. Mod. Phys.* **1968**, *40*, 441–507.
(100) Casida, M. E. Recent Advances in Density Functional Methods. In *Recent Advances in Computational Chemistry*Chong, D. P., Ed.; World Scientific: River Edge, NJ, 1995; Vol. I, Part 1, Chapter 5, pp 155−192.
(101) In eq 4 of ref 2, we erroneously stated that $\Sigma_{n>0} f_{0\rightarrow n} = 1$ for TD-DFT calculations, but in fact the exact TRK sum rule, eq 8 of this work, is preserved in TD-DFT if the basis set is complete.[100] This erroneous equation aside, what we were trying to emphasize in the discussion appearing in ref 2 is that the excitations in adiabatic, linear-response TD-DFT are strictly *one-electron* transitions, albeit "dressed" by electron correlation. True doubly excited states are absent within the adiabatic approximation.[102]
(102) Elliott, P.; Goldson, S.; Canahui, C.; Maitra, N. T. *Chem. Phys.* **2011** , DOI: 10.1016/j.chemphys.2011.03.020.
(103) For example, a TD-HF/aug-cc-pV5Z calculation of $H_2$ affords $\Sigma_{n>0} f_{0\rightarrow n} = 1.9961$. For the TD-LRC-$\mu$BOP/6-31+G* calculations that are employed here, a calculation of all excited states of $H_2O$ affords $\Sigma_{n>0} f_{0\rightarrow n} = 8.5895$, while for $H_2O^-$ we obtain $\Sigma_{n>0} f_{0\rightarrow n} = 9.2894$. For these two cases, the basis set error in the TRK sum rule is about 15%.
(104) Bernasconi, L.; Sprik, M.; Hutter, J. *J. Chem. Phys.* **2003**, *119*, 12417–12431.
(105) Neugebauer, J.; Louwerse, M. J.; Baerends, E. J.; Wesołowski, T. A. *J. Chem. Phys.* **2005**, *122*, 094115:1−−13.
(106) Lange, A.; Herbert, J. M. *J. Chem. Theory Comput.* **2007**, *3*, 1680–1690.
(107) Tawada, Y.; Tsuneda, T.; Yanagisawa, S.; Yanai, T.; Hirao, K. *J. Chem. Phys.* **2004**, *120*, 8425–8433.
(108) Vydrov, O. A.; Scuseria, G. E. *J. Chem. Phys.* **2006**, *125*, 234109:1–9.
(109) Chai, J.-D.; Head-Gordon, M. *J. Chem. Phys.* **2008**, *128*, 084106:1–15.
(110) Lange, A. W.; Rohrdanz, M. A.; Herbert, J. M. *J. Phys. Chem. B* **2008**, *112*, 6304–6308.
(111) Rohrdanz, M. A.; Martins, K. M.; Herbert, J. M. *J. Chem. Phys.* **2009**, *130*, 054112:1–8.
(112) Baer, R.; Livshits, E.; Salzner, U. *Annu. Rev. Phys. Chem.* **2010**, *61*, 85–109.
(113) We use the nomenclature for LRC functionals that is suggested in footnote 46 of ref 114, which is consistent with the usage in the Q-Chem program.[115]
(114) Richard, R. M.; Herbert, J. M. *J. Chem. Theory Comput.* **2011**, *7*, 1296–1306.
(115) Shao, Y.; Fusti-Molnar, L.; Jung, Y.; Kussmann, J.; Ochsenfeld, C.; Brown, S. T.; Gilbert, A. T. B.; Slipchenko, L. V.; Levchenko, S. V.; O'Neill, D. P., Jr.; et al. *Phys. Chem. Chem. Phys.* **2006**, *8*, 3172–3191.
(116) Tsuneda, T.; Suzumura, T.; Hirao, K. *J. Chem. Phys.* **1999**, *110*, 10664–10678.
(117) Iikura, H.; Tsuneda, T.; Yanai, T.; Hirao, K. *J. Chem. Phys.* **2001**, *115*, 3540–3544.
(118) Becke, A. D. *Phys. Rev. A* **1988**, *38*, 3098–3100.
(119) In the original VEBE benchmarking of the LRC-$\mu$BOP functional,[66,90] the Coulomb attenuation parameter was set to $\mu = 0.33\ a_0^{-1}$, whereas our TD-DFT calculations use $\mu = 0.37\ a_0^{-1}$. As documented in ref 2 and in section 4.4, the results obtained with these two different values of $\mu$ are quite similar.
(120) Hirata, S.; Head-Gordon, M. *Chem. Phys. Lett.* **1999**, *314*, 291–299.
(121) Rohrdanz, M. A.; Herbert, J. M. *J. Chem. Phys.* **2008**, *129*, 034107:1–9.
(122) Golden, S.; Tuttle, T. R., Jr. *J. Chem. Soc., Faraday Trans. 2* **1979**, *4*, 474–484.
(123) The derivation of eq 10 involves several approximations. As argued in ref 122, however, these are not expected to be numerically significant for $e^-$(aq) in the infinite-dilution limit at $T = 300$ K.
(124) Tuttle, T. R., Jr.; Golden, S. *J. Chem. Soc., Faraday Trans. 2* **1981**, *77*, 873–888.
(125) Jou, F.-Y.; Freeman, G. R. *Can. J. Chem.* **1979**, *57*, 591–597.
(126) Jou, F.-Y.; Freeman, G. R. *J. Phys. Chem.* **1979**, *83*, 2383–2387.
(127) Song, J.-W.; Hirosawa, T.; Tsuneda, T.; Hirao, K. *J. Chem. Phys.* **2007**, *126*, 154105:1–7.
(128) Becke, A. D. *J. Chem. Phys.* **1993**, *98*, 5648–5652.
(129) Lee, C.; Yang, W.; Parr, R. G. *Phys. Rev. B* **1988**, *37*, 785–789.
(130) Sommerfeld, T.; Gardner, S. D.; DeFusco, A.; Jordan, K. D. *J. Chem. Phys.* **2006**, *125*, 174301:1–7.
(131) Xu, J.; Jordan, K. D. *J. Phys. Chem. A* **2010**, *114*, 1364–1366.
(132) Wu, Y.; Tepper, H. L.; Voth, G. A. *J. Chem. Phys.* **2006**, *124*, 024503:1–12.
(133) Schwartz, B. J.; Rossky, P. J. *Phys. Rev. Lett.* **1994**, *72*, 3282–3285.
(134) Schwartz, B. J.; Rossky, P. J. *J. Chem. Phys.* **1994**, *101*, 6917–6926.